Journal of Power Sources 183 (2008) 471–478

Contents lists available at ScienceDirect

Journal of Power Sources

journal homepage: www.elsevier.com/locate/jpowsour

Synthesis and assessment of $La_{0.8}Sr_{0.2}Sc_yMn_{1-y}O_{3-\delta}$ as cathodes for solid-oxide fuel cells on scandium-stabilized zirconia electrolyte

Hongxia Gu [a], Yao Zheng [a], Ran Ran [a], Zongping Shao [a,*], Wanqin Jin [a], Nanping Xu [a], Jeongmin Ahn [b]

[a] State Key Laboratory of Materials-Oriented Chemical Engineering, College of Chemistry and Chemical Engineering, Nanjing University of Technology, No. 5 Xin Mofan Road, Nanjing, 210009, PR China
[b] School of Mechanical and Materials Engineering, Washington State University, Sloan 217, Pullman, WA 99164-2920, USA

ARTICLE INFO

Article history:
Received 6 May 2008
Accepted 20 May 2008
Available online 27 May 2008

Keywords:
$La_{0.8}Sr_{0.2}Sc_yMn_{1-y}O_{3-\delta}$
Stabilized zirconia
Solid-oxide fuel cell
Cathode

ABSTRACT

Perovskite-type $La_{0.8}Sr_{0.2}Sc_yMn_{1-y}O_{3-\delta}$ oxides (LSSM*y*, $y = 0.0$–0.2) were synthesized and investigated as cathodes for solid-oxide fuel cells (SOFCs) containing a stabilized zirconia electrolyte. The introduction of Sc^{3+} into the B-site of $La_{0.8}Sr_{0.2}MnO_{3-\delta}$ (LSM) led to a decrease in the oxides' thermal expansion coefficients and electrical conductivities. Among the various LSSM*y* oxides tested, LSSM0.05 possessed the smallest area-specific cathodic polarization resistance, as a result of the suppressive effect of Sc^{3+} on surface SrO segregation and the optimization of the concentration of surface oxygen vacancies. At 850 °C, it was only ~0.094 Ω cm^2 after a current passage of 400 mA cm^{-2} for 30 min, significantly lower than that of LSM (~0.25 Ω cm^2). An anode-supported cell with a LSSM0.05 cathode demonstrated a peak power density of 1300 mW cm^{-2} at 850 °C. The corresponding value for the cell with LSM cathode was 450 mW cm^{-2} under the same conditions. The LSSM0.05 oxide may potentially be a good cathode material for IT-SOFCs containing doped zirconia electrolytes.

1. Introduction

Fuel cells are an attractive power generation technology characterized by high energy-conversion efficiency and low emissions. Solid-oxide fuel cells (SOFCs) are all-solid-state devices and typically operate at high temperatures of 500–1000 °C [1–3]. Compared to low-temperature fuel cells, such as polymer-electrolyte-membrane fuel cells, SOFCs have superior fuel flexibility and fast electrode reaction kinetics [4–6].

Currently, yttrium or scandium stabilized zirconia are still the most commonly used SOFC electrolytes due to their excellent mechanical properties, their favorable redox stabilities, and their acceptable ionic conductivities [7–11]. Although these materials' ionic conductivities are lower than those of doped ceria (i.e. samaria doped ceria) or lanthanum gallate (i.e., $La_{0.8}Sr_{0.2}Ga_{0.8}Mg_{0.2}O_{2.9}$), the resistance that these thin-film stabilized zirconia electrolytes contribute is still acceptable at intermediate temperatures [12,13]. If the electrolyte thickness can be reduced to 5–10 μm, SOFCs equipped with either yttria-stabilized zirconia (YSZ) or scandia-stabilized zirconia (ScSZ) electrolytes are capable of supplying applicable power densities at operating temperatures as low as 650 and 600 °C, respectively. The reduction of oxygen has a high activation energy, so cathodic polarization resistance increases sharply with decreases in operating temperature. A high-performance cathode is therefore an essential component of intermediate-temperature (IT)-SOFCs. This study aims to develop novel cathode materials for IT-SOFCs containing stabilized zirconia electrolytes.

An ideal cathode for IT-SOFCs should have high electrocatalytic oxygen-reduction activity, a thermal expansion coefficient (TEC) that is compatible with that of the electrolyte, high chemical and structural stability, and low reactivity towards the electrolyte under operating conditions. $La_{0.8}Sr_{0.2}MnO_{3-\delta}$ (LSM) is one of the most frequently used cathode materials in SOFCs containing YSZ/ScSZ electrolytes because the material possesses an appropriate TEC and favorable chemical compatibility. LSM, however, has negligible oxygen ionic conductivity, and oxygen reduction is strictly limited to the electrolyte–electrode-gas triple-phase boundary (TPB) [14]. Decreasing the operating temperature drastically increases the cathodic polarization resistance to values so large that LSM does not act as a cathode at temperatures lower than 800 °C. Lanthanum cobaltite and related perovskite oxides have shown initial promise as cathodic materials for IT-SOFCs containing doped ceria electrolytes such as samaria doped ceria [15–17]. The anion and electron conductivities of such materials at reduced temperatures are sufficiently high that the active electrochemical reaction is not restricted solely to the TPB, but can exploit the entire cathode–gas interface. Unfortunately, these materials do not perform as well with stabilized zirconia electrolytes [18,19]. At high temperatures,

* Corresponding author. Tel.: +86 25 83587722; fax: +86 25 83365813.
E-mail address: shaozp@njut.edu.cn (Z. Shao).

0378-7753/$ – see front matter © 2008 Elsevier B.V. All rights reserved.
doi:10.1016/j.jpowsour.2008.05.053

the lanthanum cobaltite cathode reacts with the stabilized zirconia electrolyte to form an electrically insulating layer of $La_2Zr_2O_7$. This, of course, increases the electrode–electrolyte interfacial polarization resistance. In addition, lanthanum cobaltite has a much higher TEC than stabilized zirconia [20]. The low chemical stability of these materials might also be a drawback [21].

Doping has been widely applied to modify the properties of LSM. We have demonstrated that Sc^{3+} is an excellent dopant for cobalt-based perovskites [22,23]. In this study, we investigated the synthesis of new perovskite-type scandia-doped LSM oxides and investigated potential applications for these materials as the cathodes of IT-SOFCs containing a ScSZ electrolyte. The phase structure, electrical conductivity, thermal expansion coefficient, cathodic polarization resistance, and single-cell SOFC performance of these oxides was systematically studied.

2. Experimental

2.1. Preparation of LSSMy powders

LSSM*y* composite oxides ($y = 0.0$–0.2) were synthesized via an EDTA-citrate complexing sol–gel process [24,25]. $La(NO_3)_3$, $Sr(NO_3)_2$, $Mn(CH_3COO)_2{\cdot}4H_2O$, and Sc_2O_3 (all A.R. grade) were used as the raw materials. Sc_2O_3 powder was first dissolved in nitric acid and heated, and $Sr(NO_3)_2$, $La(NO_3)_3$, and $Mn(CH_3COO)_2{\cdot}4H_2O$ were then added. EDTA and citric acid were added to the mixture in sequence, and both acted as complexing agents. The pH of the solution was adjusted to ~6 via addition of $NH_3{\cdot}H_2O$. After evaporating the water from the mixture via heating, a transparent purple gel was obtained. The gel was pre-fired at 250 °C forming a solid precursor, which was subsequently calcinated at 1000 °C for 5 h under an air atmosphere to yield the final desired product.

2.2. Electrochemical characterization

Electrochemical characterization of these LSSM*y* cathode materials was conducted using a three-electrode electrochemical cell (Fig. 1). Electrolyte disks were prepared from $(Sc_2O_3)_{0.1}(ZrO_2)_{0.9}$ (ScSZ) powder by die-pressing. The disks were then sintered at 1500 °C for 5 h under an air atmosphere. The thickness and diameter of a sintered disk was ~0.3 and 16 mm, respectively. A cathode slurry was sprayed onto each side of the electrolyte substrate such that application was as symmetric as possible. The substrate was then calcinated at 1150 °C for 2 h under an air atmosphere to yield both the working and the counter electrodes. A reference electrode composed of silver paste (DAD-87, Shanghai Research Institute of Synthetic Resins, Shanghai, China) was painted in a ring around the counter electrode. The gap between the counter and the reference electrodes was ~4 mm. The areas of the working, the counter, and the reference electrodes were 0.26, 0.26, and 0.3 cm^2, respectively.

Cathodic polarization resistance (R_p) was measured via electrochemical impedance spectrum (EIS) measurement using a Solartron 1260A frequency response analyzer in combination with a Solartron 1287 potentiostat/galvanostat. The frequency range of EIS measurements was from 0.1 Hz to 100 kHz, and the signal amplitude was 10 mV. Data were collected using ZPlot 2.9c software. Measurements were conducted both with and without a current polarization treatment in which the electrodes were subjected to 400 mA cm^{-2} of current for 30 min. Cathodic overpotential was measured using a Solartron 1287 potentiostat/galvanostat, which was operated via Corrware 2.9c software. The polarization current density was varied from 0 to 400 mA cm^{-2} in 20 mA cm^{-2} intervals. Post-factum correction of the cyclic voltammetry (CV) results was applied to correct for the IR drop corresponding to the electrolyte and lead resistances, thereby establishing resistance-free *I*/*E* characteristics. The series resistance data obtained from EIS measurements was used to make this correction.

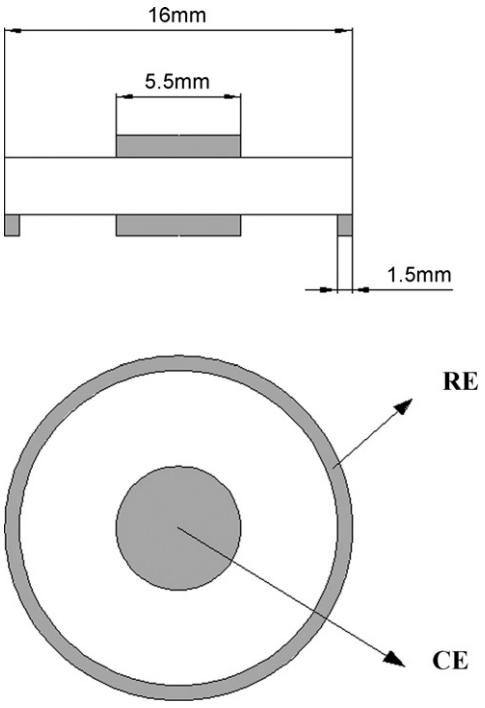

Fig. 1. A schematic of the three-electrode system, CE: counter electrode; RE: reference electrode.

2.3. Single-cell testing

High-energy ball milling (FRITSCH, Pulverisette 6) was employed to prepare anodic powder composed of 60 wt% NiO and 40 wt% ScSZ. The electrolyte membrane was deposited onto the NiO + ScSZ substrate using a dual-dry-pressing technique and subsequent co-firing at 1500 °C for 5 h under an air atmosphere. This aimed in densifying the electrolyte layer and enhancing the adhesion between the two layers. A cathode slurry containing LSSM*y* ($y = 0.0$–0.2) was sprayed onto the electrolyte surface and then calcinated at 1150 °C for 2 h under an air atmosphere. Silver paste was used as the current collector. A four-terminal configuration was used during the single cell tests. Fuel cell performance at temperatures between 650 and 850 °C was assessed via *I*–*V* characterization. Measurements were performed using a digital source meter (Keithley 2420) that was interfaced with a computer to facilitate data acquisition.

2.4. Other characterization

The phase structures of the oxide materials were investigated by X-ray diffraction using a Bruker D8 Advance Diffractometer. Diffraction patterns were collected at room temperature by step scanning angles (2θ) between 10° and 90°. The morphological features of the prepared cells were examined with an environmental scanning electron microscope (ESEM, QUANTA-2000). The thermal expansion coefficient (TEC) was measured using a Netsch DIL 402C/3/G dilatometer, which operated between room temperature and 1000 °C with an air purge flow rate of 50 ml min^{-1} (STP, standard temperature and pressure). The oxide's electrical conductivity was measured using a four-probe DC conductivity instrument. Prepared powders were ball-milled and subsequently pressed into

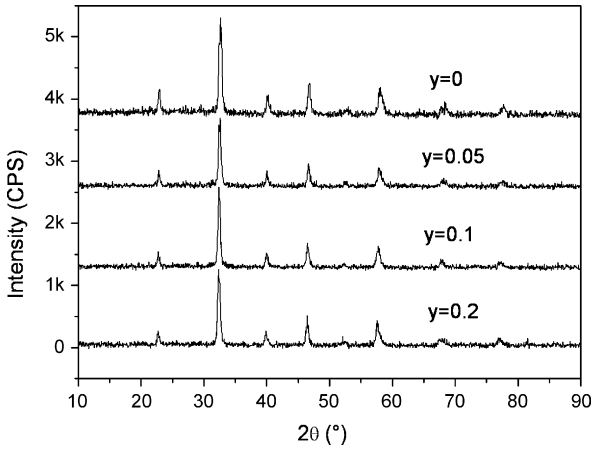

Fig. 2. X-ray diffraction patterns of $La_{0.8}Sr_{0.2}Sc_yMn_{1-y}O_{3-\delta}$ (y = 0.0–0.2) obtained from the calcination of their sol–gel precursors at 1000 °C for 5 h under an air atmosphere.

green bars (5 mm × 8 mm × 25 mm) with stainless steel dies under a hydraulic load of 30 tons. The green bars were densified by sintering at 1300 °C for 5 h, silver paste electrodes were applied to each of the bars, and four wires were attached to the edges of the bar as current and voltage probes. Measurements were conducted at intervals of 10 °C from 300 to 900 °C using a Keithley 2420 source meter.

3. Results and discussion

3.1. Basic characterization

The room-temperature X-ray diffraction (XRD) patterns were obtained for each of the LSSM*y* oxides prepared with varying Sc^{3+} doping concentrations (y = 0.0–0.2) (Fig. 2). For all LSSM*y* samples, the diffraction peaks indexed well to perovskite structures with orthorhombic symmetry. This suggested that Sc^{3+} was successfully incorporated into the B-site (manganese site) of the LSM lattice. In addition, each LSSM*y* oxide's set of lattice parameters was calculated (Table 1). The lattice constant increased with increasing Sc^{3+} doping concentration, and this result coincided with the larger ionic radius of Sc^{3+} (0.745 Å) compared to Mn^{3+} (0.645 Å) and Mn^{4+} (0.53 Å).

The high-temperature phase reaction between LSSM*y* and ScSZ was examined by mixing them in a 50:50 weight ratio in the powder state, followed by calcinations at various temperatures for 5 h in air (XRD not shown). Only weak additional diffraction peaks indexed to the $La_2Zr_2O_7$ phase were observed at a calcination temperature of 1150 °C for LSSM*y*, while the reaction was negligible at a temperature of 1100 °C or lower. Considering the calcination at 1150 °C made better adhesion of the cathode layer to the electrolyte surface, it was selected for fabricating the electrode onto electrolyte surface. Detailed examination of the effect of the phase reaction on the electrode performance is not referenced in this study, but will be conducted in the future.

Table 1
Lattice parameters of $La_{0.8}Sr_{0.2}Sc_yMn_{1-y}O_{3-\delta}$ (y = 0.0–0.02) oxides in air.

Sample	Cell parameters			
	a (Å)	b (Å)	c (Å)	V (Å^3)
$La_{0.8}Sr_{0.2}MnO_{3-\delta}$	5.357	5.796	7.130	221.38
$La_{0.8}Sr_{0.2}Sc_{0.05}Mn_{0.95}O_{3-\delta}$	5.364	5.810	7.145	222.69
$La_{0.8}Sr_{0.2}Sc_{0.1}Mn_{0.9}O_{3-\delta}$	5.385	5.848	7.151	225.17
$La_{0.8}Sr_{0.2}Sc_{0.2}Mn_{0.8}O_{3-\delta}$	5.395	5.844	7.175	226.23

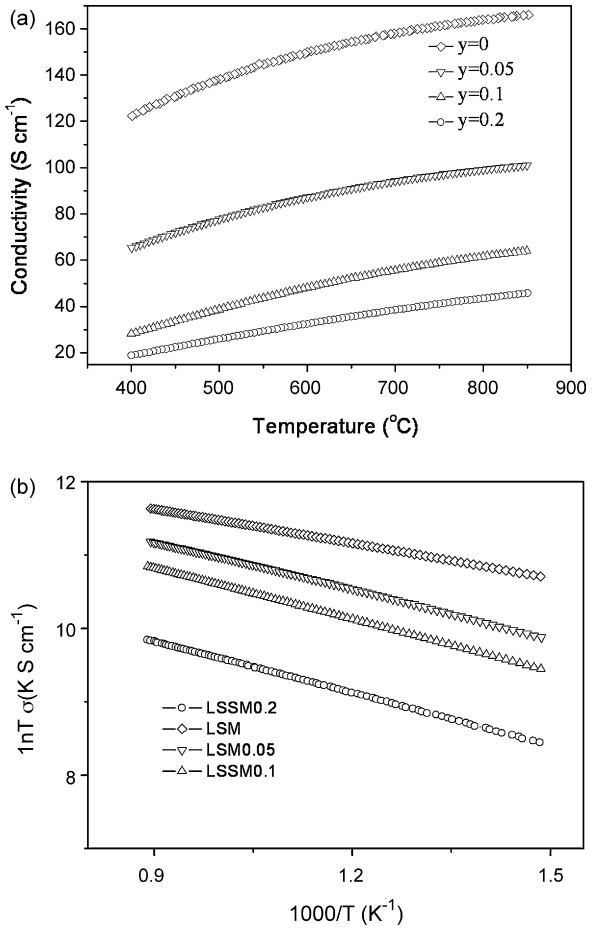

Fig. 3. The temperature dependence of electrical conductivities of $La_{0.8}Sr_{0.2}Sc_yMn_{1-y}O_{3-\delta}$ (y = 0.0–0.2) oxides under an air atmosphere in Arrhenius plots.

Matching the thermal expansion coefficient of the electrode to that of the electrolyte is crucial to the fuel cell's long-term stability during thermal cycling. Between room temperature and 1000 °C, the various LSSM*y* oxides possessed TECs of 12.4×10^{-6}, 12.7×10^{-6}, 11.0×10^{-6}, and 11.0×10^{-6} K^{-1} for y values of 0.0 (LSM), 0.05 (LSSM0.05), 0.1 (LSSM0.1), and 0.2 (LSSM0.2), respectively. The measured TEC of LSM matched the values published in the literature [26]. Both LSSM0.1 and LSSM0.2 possessed TECs smaller than LSM, implying that these materials were more compatible with the stabilized zirconia electrolyte than LSM [27]. The differences in TEC among the various LSSM*y* oxides were sufficiently small, so that any one of these materials was suitable in terms of its thermal expansion properties for application in cathodes adhering to stabilized zirconia electrolyte.

Substitution of a lower oxidation state cation, such as Sr^{2+}, for the La^{3+} in the A-site of $LaMnO_3$ would create an electrical charge imbalance. Either an increase in the B-site metal ion's oxidation state (i.e. $Mn^{3+} \rightarrow Mn^{4+}$), or the formation of oxygen vacancies ($V_O^{\bullet\bullet}$) in the lattice structure must occur to compensate for this imbalance. In the case of LSM, the former phenomenon plays a larger role in restoring electrical charge balance. Electrical conduction occurs as electron hopping between the multivalent B-site metal ions. The total electrical conductivity of LSSM*y* was measured as a function of scandium doping concentration using the four-probe DC method (Fig. 3). The increased electrical conductivity with increasing operating temperature verified the LSSM*y* oxides' putative semi-conductor properties. Increasing the Sc^{3+}

doping concentration decreased the total conductivity, especially at higher dopant concentrations. For example, LSM demonstrated an electrical conductivity of 166 S cm^{-1} at 850 °C, which was similar to the literature value [26], but LSSM0.2 demonstrated an electrical conductivity only of ~46 S cm^{-1} at the same temperature. The temperature dependence of electrical conductivity was fitted to the equation $\sigma = A_0/T \exp(-E_a/kT)$, where σ is the electrical conductivity (S cm^{-1}), T is the temperature (K), E_a is the activation energy (J), k is the Boltzmann constant (J K^{-1}), and A_0 is the pre-exponential factor (S K cm^{-1}). The activation energies of electron transport for the various LSSMy oxides were 12.69 ± 0.02, 13.34 ± 0.11, 18.48 ± 0.03, and 19.48 ± 0.06 kJ mol^{-1} for y values of 0.0, 0.05, 0.1, and 0.2, respectively.

The electrical conductivity measured by four-probe DC method is a sum of electronic and oxygen ionic conductivity. We have tried to obtain the oxygen ionic conductivity of LSSMy by the oxygen permeation measurement of LSSMy membrane. Within the experimental errors, the oxygen permeation flux through LSSMy membranes between 600 and 900 °C is negligible, suggesting the Sc^{3+} doping did not introduce oxygen ionic conductivity into the oxide under zero current polarization. Therefore, the measured electrical conductivity represents the electronic conductivity.

For the perovskite oxide, the electronic conductivity is closely related with its phase structure and the characteristics of the variable metal ion(s) at the B-site. Since the same phase structure was observed for all LSSMy oxides with varied Sc^{3+} doping amounts, the effect of lattice structure on the electrical conductivity can be reasonably assumed to be negligible. The electron conduction in perovskite is created by B-site lattice cations through strongly overlapping B–O–B bonds with a mechanism like the Zerner double exchange process shown below:

$$B^{n+}\text{–}O^{2-}\text{–}B^{(n+1)+} \Rightarrow B^{(n+1)+}\text{–}O^{-}\text{–}B^{(n+1)+} \Rightarrow B^{(n+1)+}\text{–}O^{2-}\text{–}B^{n+}$$

Due to the constant valence state of Sc^{3+}, it is impossible for electron conduction through the overlapping of 2p of oxygen with the 3d orbital of Sc^{3+}. Therefore, Sc^{3+} acted as a block for electron conduction. This explains the decrease in electrical conductivity with the increase of Sc^{3+} doping level and the increase of activation energy for electrical conduction. Interestingly, the activation energy increased greatly from $y = 0.05$ to 0.1, but only slightly from $y = 0.0$ to 0.05. Thus, the blocking effect was significant only for oxides with $y \geq 0.1$. In fuel cell applications, over-doping with Sc^{3+} may introduce current collecting problems stemming from low electrical conductivity. A smaller Sc^{3+} doping concentration was preferred for this reason.

3.2. Electrochemical performance of LSSMy without DC polarization

The EIS of freshly prepared LSSMy ($y = 0.0$–0.2) electrodes that had not been activated with DC treatment were acquired (Fig. 4). All measured values were too large for these materials to be appropriate cathode materials. This suggested that Sc^{3+} doping did not facilitate ionic conduction into the bulk oxide in the absence of direct current polarization treatments, agreeing well with the oxygen permeation measurement of corresponding dense membranes. In other words, the oxygen reduction reaction occurred primarily at the TPB. A modest reduction in the area-specific polarization resistance relative to that of LSM was nevertheless observed for the LSSM0.05 oxide, and this suggested that Sc^{3+} doping may promote surface oxygen reduction chemistry. Oxygen reduction over SOFC cathode proceeds via a complex mechanism, which involves the gaseous diffusion of molecular oxygen to the electrode, the adsorption of oxygen onto the electrode surface, the atomic

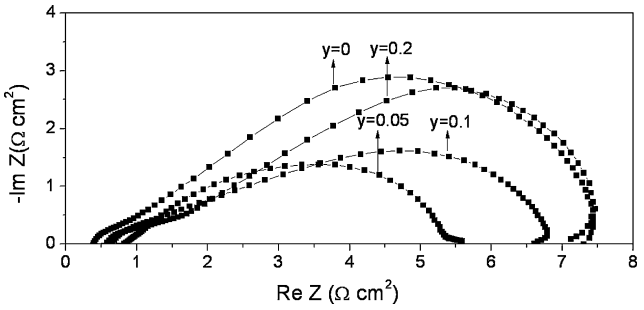

Fig. 4. Cathodic polarization resistances of freshly prepared $La_{0.8}Sr_{0.2}Sc_yMn_{1-y}O_{3-\delta}$ ($y = 0.0$–0.2) at 850 °C without DC polarization treatment.

dissociation of dioxygen, the migration of dissociated, adsorbed oxygen intermediates/ions to the reduction zone, charge transfer, and the incorporation of oxide ions into the electrolyte lattice at the TPB. The diffusion of oxygen species along the electrode surface to the electrode/electrolyte interface normally occurs at low frequency and is frequently the rate-limiting step. In addition, there is significant evidence of strontium enrichment on the $La_xSr_{1-x}MnO_{3-\delta}$ and $La_xSr_{1-x}Co_yFe_{1-y}O_{3-\delta}$ electrode surfaces in air from XPS and neutron powder diffraction experiments [28–30]. Since SrO is an insulator, its presence blocks the oxygen diffusion pathway and inhibits surface diffusion. The effect of the Sc^{3+} doping concentration on surface SrO enrichment was investigated with pH measurements. About 0.002 mol LSSMy ($y = 0.0$–0.2) powder was boiled in 0.2 l de-ionized water for 2 h to dissolve the SrO before it was cooled to ~30 °C. The solution's pH was then measured with a digital pH meter. The oxide solutions' pH values were measured at 9.0, 8.7, 8.6, and 8.3 for y values of 0.0, 0.05, 0.1, and 0.2, respectively. Because SrO is basic, a higher pH value indicates a higher concentration of SrO in solution that, in turn, corresponds to a higher surface concentration on the LSSMy oxide. The observed decrease in solution pH with increasing Sc^{3+} concentration implied that doping suppressed SrO generation, and this may have accounted for the superior electrochemical performance of LSSM0.05 relative to that of LSM.

Oxygen reduction, however, was also closely related to the surface concentration of oxygen vacancies, and this value depended on the concentration of surface Mn^{4+}. Previous research has demonstrated that the average oxidation state of manganese was higher on the oxide surface than in the bulk [29]. H_2 temperature-programmed reduction (TPR) was applied to measure the Mn^{4+} surface concentration of the LSSMy oxides ($y = 0.0$–0.2) (Fig. 5). The shoulder peak near 400 °C was attributed to the reduction of sur-

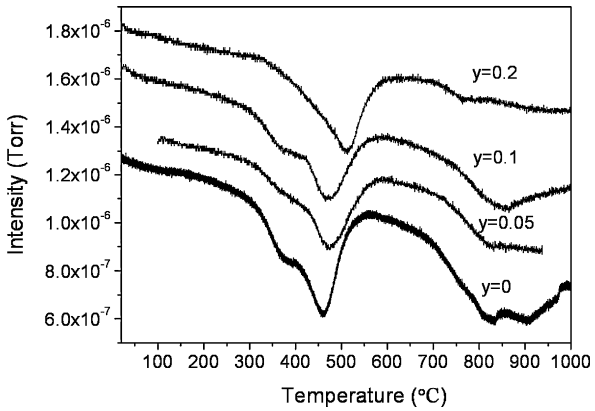

Fig. 5. Hydrogen temperature-programmed reduction curves of $La_{0.8}Sr_{0.2}Sc_y Mn_{1-y}O_{3-\delta}$ ($y = 0.0$–0.2) oxides.

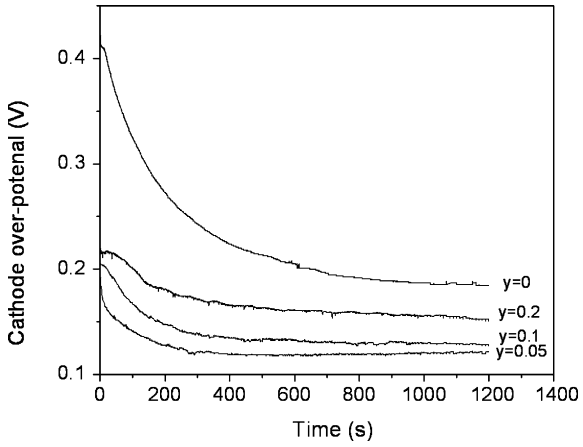

Fig. 6. A time course of the cathodic overpotential (IR corrected) of $La_{0.8}Sr_{0.2}Sc_yMn_{1-y}O_{3-\delta}$ ($y = 0.0$–0.2) oxides with a constant applied current density of 400 mA cm^{-2} at 850 °C.

face Mn^{4+} to Mn^{3+}, and the peaks at 500 and 800 °C were ascribed to the reduction of Mn^{4+} to Mn^{3+} and Mn^{3+} to Mn^{2+}, respectively, in the oxide bulk. The Sc^{3+} dopant generally suppressed surface Mn^{4+}. There was almost no reduction peak corresponding to surface Mn^{4+} reduction in the spectrum of the $y = 0.2$ oxide. The decreased Mn^{4+} surface concentration increased the surface oxygen vacancy concentration. An optimal concentration of vacancies should improve the material's electrochemical performance because these vacancies are essential to the oxygen reduction and migration processes. This may also explain the superior electrode performance of LSSM0.05 in the absence of DC polarization treatment. Because Sc^{3+} ions are much larger than both Mn^{4+} and Mn^{3+}, excessive Sc^{3+} dopant in oxide B-sites may create trapping centers for anion vacancies and thus may deteriorate the material's oxygen conductivity. Sc^{3+} doping in excess of $y = 0.05$ therefore increased the polarization resistance of LSSM*y* oxides.

3.3. LSSMy electrode performance after current polarization

It has been established that treatment of an LSM electrode with DC can minimize polarization losses [31–33]. The cathodic overpotential (IR corrected) of LSSM*y* electrodes was measured as a function of time at a polarization current density of 400 mA cm^{-2} at 850 °C (Fig. 6). The initial overpotentials were 0.430, 0.209, 0.205, and 0.225 V for LSSM*y* oxides with $y = 0.0$, 0.05, 0.1, and 0.2, respectively. LSM had a much larger initial overpotential than all LSSM*y* oxides ($y > 0.0$). This result agreed well with the high SrO and Mn^{4+} surface concentrations of LSM that were observed in our previous experiments. The larger initial overpotential of LSSM0.2 compared to LSSM0.05 or LSSM0.1 was attributed to the Sc^{3+} trapping effect, which immobilized the surface oxygen vacancies.

All samples experienced a sharp decrease in overpotential after the first several minutes of polarization, and this corresponded to the successful creation of oxygen vacancies and the dissolution of surface SrO into the electrode bulk. The elimination of SrO via DC treatment was previously demonstrated [32,33]. The SrO-free surface allowed faster surface exchange kinetics, which contributed in part to the enhanced electrode performance. The formation of oxygen vacancies in the bulk allowed the reduction of oxygen to occur at the electrode-gas dual-phase boundary (DPB) and allowed charge transfer to occur over the whole electrolyte–electrode dual-phase interface. This also had the effect of enhancing electrode performance. The oxides' steady-state overpotentials during treatment with

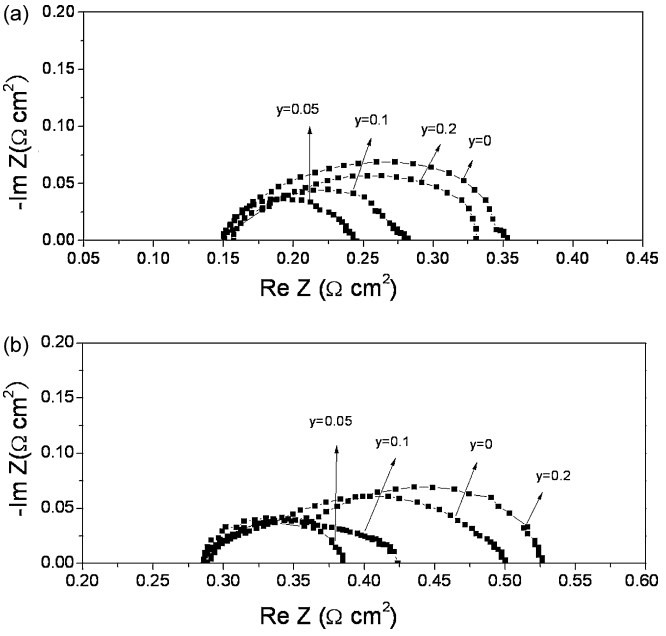

Fig. 7. EIS of $La_{0.8}Sr_{0.2}Sc_yMn_{1-y}O_{3-\delta}$ ($y = 0.0$–0.2) electrodes during exposure to a current density of 400 mA cm^{-2} acquired 30 min after the onset of current application at (a) 850 °C; (b) 800 °C.

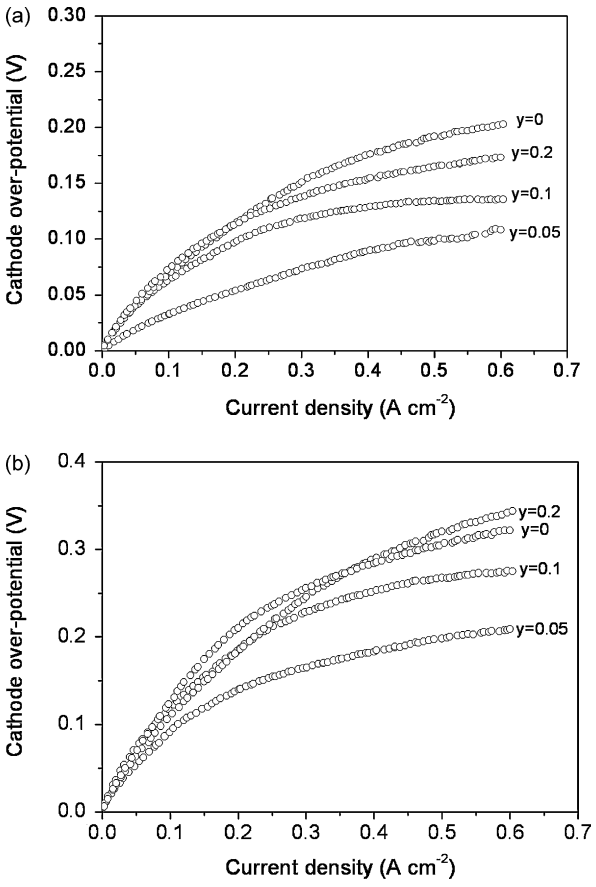

Fig. 8. The polarization current density dependence of the overpotential for $La_{0.8}Sr_{0.2}Sc_yMn_{1-y}O_{3-\delta}$ ($y = 0$–0.2) electrodes at (a) 850 °C; (b) 800 °C.

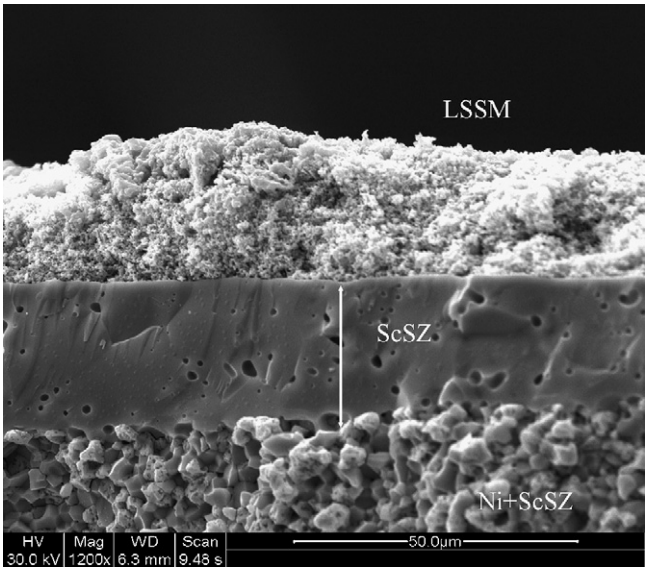

Fig. 9. SEM image of the cross-section of a typical ScSZ + Ni supported thin-film ScSZ electrolyte solid-oxide fuel cell with an LSSM cathode.

400 mA cm^{-2} polarization current were ranked as follows: LSM (0.185 V) > LSM0.2 (0.151 V) > LSM0.1 (0.132 V) > LSM0.05 (0.120 V). Under current polarization conditions, LSSM0.05 showed the best performance, and the overall trend among the oxides was the same as that without current polarization (Fig. 4). The drop in overpotential from initial value to steady-state was 0.244, 0.089, 0.073, and 0.074 V for LSSMy with y = 0.0, 0.05, 0.1 and 0.2, respectively. The decrease in voltage drop observed for increasing Sc^{3+} doping concentration was attributed to the effect of Sc^{3+} on suppressing variations in the bulk (i.e., oxygen vacancies) and surface properties (i.e. SrO accumulation).

The EIS of all LSSMy oxides (y = 0.0–0.2) were obtained at 800 and 850 °C with current polarization (400 mA cm^{-2}) measured 30 min after the onset of DC application (Fig. 7). For all samples, the electrode polarization resistance decreased considerably under current polarization conditions, and LSSM0.05 showed the lowest area-specific polarization resistance (~0.094 Ω cm^2) at 850 °C. At the same temperature, the corresponding value for LSM was ~0.25 Ω cm^2. Increasing Sc^{3+} doping concentration such that $y \geq 0.05$, however, resulted in a rebound of polarization resistance. This reversal was attributed to defect association between Sc^{3+} and the oxygen vacancies in the LSSMy bulk because higher doping concentrations should have increased the significance of these defect associations. The LSSM0.2 oxide demonstrated both higher and lower area-specific polarization resistance values than LSM at 800 and 850 °C, respectively.

The dependence of overpotential on polarization current density varied with Sc^{3+} doping concentration (Fig. 8). At 850 °C, the LSSMy overpotentials were ranked as follows: LSSM0.05 < LSSM0.1 < LSSM0.2 < LSM. At 800 °C, the ranking was the same, except the overpotential of LSSM0.2 was larger than that of LSM. These observations coincided with the previous impedance measurements.

We noticed during the overpotential measurements that the cathodes' polarization resistances were somewhat larger than those obtained during impedance measurements. This suggested

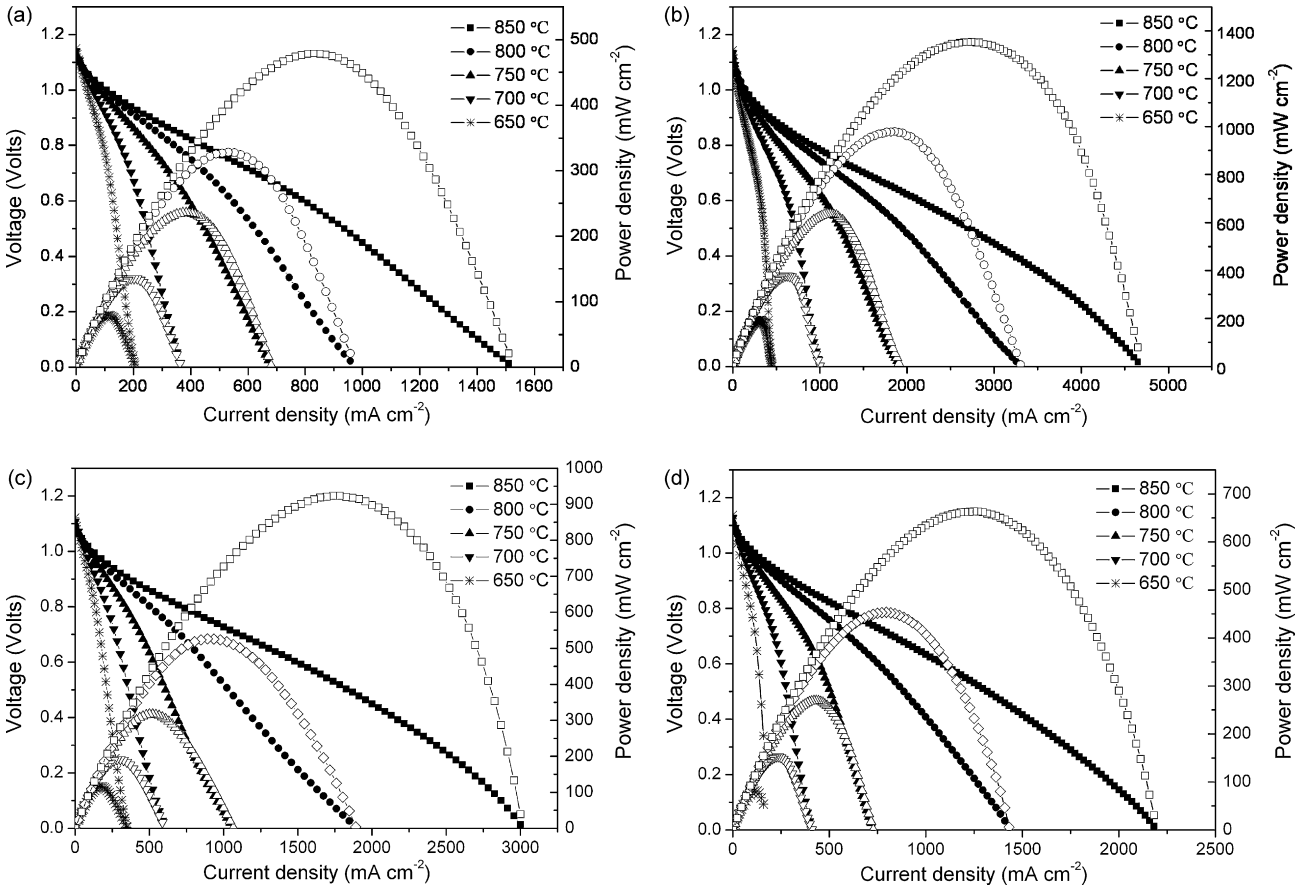

Fig. 10. I–V polarization curves for ScSZ + Ni supported thin-film ScSZ fuel cells equipped with $La_{0.8}Sr_{0.2}Sc_yMn_{1-y}O_{3-\delta}$ cathodes measured at different temperatures using H_2 as fuel: (a) y = 0.0; (b) y = 0.05; (c) y = 0.1; (d) y = 0.2.

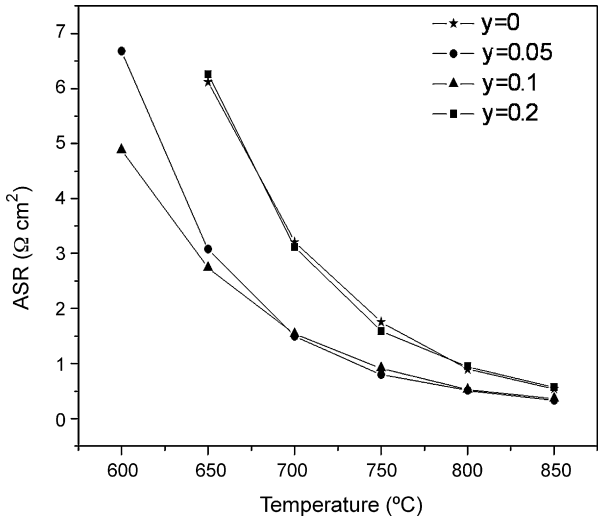

Fig. 11. The area-specific resistances (ASRs) of $La_{0.8}Sr_{0.2}Sc_yMn_{1-y}O_{3-\delta}$ cathodes with varied Sc^{3+} doping concentrations under OCV conditions.

that there was interfacial resistance between the current collector and the cathode layer, because current collection efficiency was insufficient. Similar phenomena were also observed by Jiang et al. [34]. Regardless, it was evident that cathode performance was significantly improved by slight Sc^{3+} doping.

3.4. Single-cell performance

Anode-supported fuel cells containing ScSZ thin-film electrolyte were fabricated to test the performance of LSM*y* oxides as cathode materials under typical SOFC operating conditions. Fuel cell performance is closely related not only to electrode composition, but also to electrode microstructure. To ensure a reasonable comparison of the different materials, our fabrication techniques were rigorously optimized to minimize any variations in the microstructures of both the electrodes and the electrolyte. Dual dry-pressing, which is an elegant, reproducible, and simple technique, was used to fabricate anode-supported thin-film SOFCs. A typical cell's cross-section was imaged via SEM revealing an ScSZ + Ni supported thin-film ScSZ electrolyte roughly 30 μm thick and an LSM*y* cathode 30–40 μm thick (Fig. 9). In addition, the fuel cell cathodes all adhered nicely to their respective electrolyte layers, thereby lowering the polarization resistance of their interfaces.

Fuel cell performance was assessed via the *I*–*V* polarization method. The cathode atmosphere was ambient air, and H_2 fuel was flowed over the anode at a rate of 80 ml min^{-1} (STP). The cells' current–voltage characteristics and power densities were measured at different temperatures (Fig. 10). The open-circuit voltages (OCVs) for wet H_2 were close to the values predicted by the Nernst equation, suggesting efficient cell sealing. The maximum power densities of the fuel cell equipped with an LSM cathode were ~450, ~200, and ~80 mW cm^{-2} at 850, 750, and 650 °C, respectively. The respective values for the cell equipped with an LSM0.05 cathode were ~1300, ~650, and ~200 mW cm^{-2}. Because fabrication techniques were rigorously controlled to minimize confounding variables, it was assumed that the observed differences in fuel cell performance were attributable solely to the activity of the cathode. Thus, it was concluded that doping a small concentration of Sc^{3+} into LSM increased overall fuel cell performance. The various fuel cells' area-specific electrode polarization resistances were measured under OCV conditions (Fig. 11). The reported electrochemical impedance was a combination of anode and cathode polarization resistances. Total polarization resistance decreased significantly for the $y = 0.05$ oxide. Assuming the anode polarization resistance was identical among all cells, Sc^{3+} doping ($y = 0.05$, 0.1) improved cathode performance. The best performance was achieved at a concentration between $y = 0.05$ to 0.1, which agreed with our previous three-electrode electrochemical polarization tests.

4. Conclusions

Doping Sc^{3+} into the B-site of $La_{0.8}Sr_{0.2}MnO_{3-\delta}$ formed new perovskites with the empirical formula $La_{0.8}Sr_{0.2}Sc_yMn_{1-y}O_{3-\delta}$. The oxides in which $y = 0.0$–0.2 had the same orthorhombic symmetry as the parent oxide. Introduction of Sc_2O_3 into the oxides led to decreased thermal expansion and electrical conductivity, but $La_{0.8}Sr_{0.2}Sc_{0.05}Mn_{0.95}O_{3-\delta}$ oxides still maintained acceptable electrical conductivity. Doping with Sc^{3+} also suppressed surface SrO accumulation, and this suppression facilitated oxygen surface diffusion. Among the various $La_{0.8}Sr_{0.2}Sc_yMn_{1-y}O_{3-\delta}$ oxides with different Sc^{3+} doping concentration examined, $La_{0.8}Sr_{0.2}Sc_{0.05}Mn_{0.95}O_{3-\delta}$ demonstrated the smallest area-specific polarization resistance and the lowest overpotential both with and without DC polarization treatment. Over-doping with Sc^{3+}, however, increased polarization resistance because the mismatch in ionic radius size between Sc^{3+} and $Mn^{3+/4+}$ induced defect association between Sc^{3+} and oxygen vacancies. The optimal Sc^{3+} doping concentration was found to be $y = 0.05$. At 750 °C, the fuel cell equipped with a $La_{0.8}Sr_{0.2}Sc_{0.05}Mn_{0.95}O_{3-\delta}$ cathode delivered a peak power density of ~650 mW cm^{-2}, which was more than twice that of its counterpart cell equipped with a LSM cathode (~200 mW cm^{-2}). These results suggested that $La_{0.8}Sr_{0.2}Sc_{0.05}Mn_{0.95}O_{3-\delta}$ has great potential for application as a cathode material in IT-SOFCs containing stabilized zirconia electrolyte. A composite cathode formed by mixing $La_{0.8}Sr_{0.2}Sc_{0.05}Mn_{0.95}O_{3-\delta}$ with electrolytic materials, such as YSZ or ScSZ, may increase the cathode even performance.

Acknowledgements

This work was supported by the National Natural Science Foundation of China under contract nos. 20646002 and 20676061, by National 863 program under contract no. 2007AA05Z133, and by National Basic Research Program of China under contract no. 2007CB209704. Dr. Zongping Shao also would like to acknowledge the financial support from Chinese Ministry of Education via the Program for Changjiang Scholars and Innovative Research Team in University (no. IRT0732)

References

[1] B.C.H. Steele, A. Heinzel, Nature 414 (2001) 345–352.
[2] Z.P. Shao, S.M. Haile, Nature 431 (2004) 170–173.
[3] A. Atkinson, S.A. Barnett, R.J. Gorte, J.T.S. Irvine, A.J. Mcevoy, M. Mogensen, S.C. Singhal, J.M. Vohs, Nat. Mater. 3 (2004) 17–27.
[4] S. Park, J.M. Vohs, R.J. Gorte, Nature 404 (2000) 265–267.
[5] S.B. Adler, Chem. Rev. 104 (2004) 4791–4843.
[6] Z.P. Shao, S.M. Haile, J. Ahn, P.D. Ronney, Z.L. Zhan, S.A. Barnett, Nature 435 (2005) 795–798.
[7] K. Poeppelmeier, Science 295 (2002) 1849.
[8] C.R. Xia, M.L. Liu, Adv. Mater. 14 (2002) 521–523.
[9] Y. Liu, S.W. Zha, M.L. Liu, Chem. Mater. 16 (2004) 3502–3506.
[10] S.P.S. Badwal, F.T. Ciacchi, D. Milosevic, Solid State Ionics 136–137 (2000) 91–99.
[11] K. Nomura, Y. Mizutani, M. Kawai, Y. Nakamura, O. Yamamoto, Solid State Ionics 132 (2000) 235–239.
[12] J.W. Fergus, J. Power Sources 162 (2006) 30–40.
[13] X. Guo, E. Vasco, S. Mi, K. Szot, E. Wachsman, R. Waser, Acta Mater. 53 (2005) 5161–5166.
[14] H.C. Yu, K.Z. Fung, Mater. Res. Bull. 38 (2003) 231–239.
[15] M.G. Bellino, J.G. Sacanell, D.G. Lamas, A.G. Leyva, N.E. Walsoe de Reca, J. Am. Chem. Soc. 129 (2007) 3066–3067.

[16] K.T. Lee, A. Manthiram, Chem. Mater. 18 (2006) 1621–1626.
[17] Y.L. Zhang, S.W. Zha, M.L. Liu, Adv. Mater. 17 (2005) 487–491.
[18] O. Yamamoto, Y. Takeda, R. Kanno, M. Noda, Solid State Ionics 22 (1987) 241–246.
[19] H.Y. Tu, Y. Takeda, N. Imanishi, O. Yamamoto, Solid State Ionics 117 (1999) 277–281.
[20] G.C. Kostogloudis, C. Ftikos, Solid State Ionics 126 (1999) 143–151.
[21] M. Gödickemeier, K. Sasaki, L.J. Gauckler, I. Riess, Solid State Ionics 86–88 (1996) 691–701.
[22] P.Y. Zeng, R. Ran, Z.H. Chen, W. Zhou, H.X. Gu, Z.P. Shao, S.M. Liu, J. Alloys Compd. 455 (2008) 465–470.
[23] P.Y. Zeng, R. Ran, Z.H. Chen, H.X. Gu, Z.P. Shao, S.M. Liu, AIChE J. 53 (2007) 3116–3124.
[24] W. Zhou, Z.P. Shao, W.Q. Jin, J. Alloys Compd. 426 (2006) 368–374.
[25] H.X. Gu, R. Ran, W. Zhou, Z.P. Shao, J. Power Sources 172 (2007) 704–712.
[26] A. Hammouche, E. Siebert, A. Hammou, Mater. Res. Bull. 24 (1989) 367–380.
[27] N.Q. Minh, T. Takahashi, Science and Technology of Ceramic Fuel Cells, Elsevier, Amsterdam, 1995, p. 117.
[28] S.A. Antony, K. Swaminathan, K.S. Nagaraja, O.M. Sreedharan, J. Alloys Compd. 322 (2001) 113–119.
[29] P. Decorse, G. Caboche, L.C. Dufour, Solid State Ionics 117 (1999) 161–169.
[30] N. Miura, Y. Okamoto, J. Tamaki, K. Morinaga, N. Yamazoe, Solid State Ionics 79 (1995) 195–200.
[31] F.H. Heuveln, H.J.M. Bouwmeester, J. Electrochem. Soc. 144 (1997) 134–140.
[32] W. Wang, S.P. Jiang, Solid State Ionics 177 (2006) 1361–1369.
[33] W. Wang, S.P. Jiang, J. Solid State Electrochem. 8 (2004) 914–922.
[34] S.P. Jiang, L.G. Gove, I. Apateanu, Solid State Ionics 160 (2003) 15–26.